TASK QUARTERLY 8 No 3 (2004), 423–437

ANALYSIS OF NON-LINEAR PROPERTIES OF CARDIOMYOCYTE CELLULAR MEMBRANES

KRZYSZTOF GRZĘDA[1], ANTONI NOWAKOWSKI[1]
AND PAWEŁ CZARNUL[2]

[1] *Department of Biomedical Engineering,*
Gdansk University of Technology,
Narutowicza 11/12, 80-952 Gdansk, Poland
kgrzeda@biomed.eti.pg.gda.pl, antowak@eti.pg.gda.pl

[2] *Department of Computer System Architecture,*
Gdansk University of Technology,
Narutowicza 11/12, 80-952 Gdansk, Poland
pczarnul@eti.pg.gda.pl

(Received 28 April 2004)

Abstract: Non-linear properties of cardiomyocyte membranes are poorly understood. We model a cell membrane using the Beeler-Reuter model with the Drouhard-Roberge modification (the BRDR model). Simulations are performed using AC voltage test excitation of 1 or 100 kHz frequency and 1 or 10 mV RMS. Values of currents flowing through the cell membrane are considered to be the response. The BRDR response is presented at the fundamental frequency and at its second and third harmonics. The response is mainly contributed to by the time-independent potassium current (i_{K1}) during resting membrane potential. The level of currents varies strongly during the period of action potential. However, the linear response from the membrane capacitance is relatively high. The second and third harmonics of the 1 kHz/10 mV probing voltage carry some information about the action potential. In particular, it may be used to investigate the process of repolarization and its disorders.

Keywords: cardiomyocyte membrane, electrical impedance, harmonic distortion

Nomenclature

V_m – transmembrane potential,
i_{Na} – fast sodium current,
i_{K1} – time-independent potassium current,
i_{x1} – time-dependent potassium current,
i_s – slow inward current,
i_{ion} – total ionic current,
f_x – probing signal frequency,
C_m – specific membrane capacitance,
$[\mathrm{Ca}]_{\mathrm{i}}$ – intracellular concentration of calcium ions,
ΔV_m – disturbance of the transmembrane potential,
m, h, x_1, d, f – gating variables defined in the BRDR model,

m_∞, h_∞, $x_{1\infty}$, d_∞, f_∞ – steady state values of the gating variables,
τ_m, τ_h, τ_{x1}, τ_d, τ_f – time constants associated with the gating variables.

1. Introduction

The electrical impedance of the heart is an important parameter for many medical procedures, both in clinical practice and in research. In particular, it determines current distribution during electrical defibrillation and heart pacing. At the same time, it is useful in studies of such cardiac phenomena, as ischemia [1] and hemodynamics [2].

Myocardial impedance depends on many biophysical parameters, including intra- and extracellular conductance, the ratio of membrane area to tissue volume, and the electrical properties of cellular membranes. Our present work is dedicated to the latter.

Non-linear properties of cardiomyocyte membranes have been known for many years and are described by many mathematical models, starting from the Hodgkin-Huxley formalism [3], through the Beeler-Reuter model [4] and its Drouhard-Roberge modification [5] (the BRDR model), a defibrillation version of the BRDR model (that is the BRDR model adapted by Skouibine *et al.* to handle large, non-physiological values of transmembrane potential) [6], to the most accurate Luo-Rudy models [7–9]. However, in simulations related to impedance, the membrane is usually approximated to a linear, parallel RC circuit. This leads us to the following questions:

1. How large harmonic distortion can be produced by the membrane?
2. How does the action potential influence the membrane's impedance/admittance? (Describing the membrane using admittance is more convenient since its value is proportional to the membrane's area.)
3. What test excitation should be used to detect and measure harmonic distortions?

The goal of this paper is to answer the above questions. Our approach is focused on considering the membrane as an idealised test circuit, without other factors affecting actual measurements of myocardial impedance, such as variable geometry, blood in the heart chambers, *etc.*

2. Method

2.1. Model

We model a piece of a cellular membrane using the Beeler-Reuter model [4] with the Drouhard-Roberge modification [5]. Detailed equations of the model are presented in the appendix. We assume the membrane's specific capacitance to be $1\mu\mathrm{F}\cdot\mathrm{cm}^{-2}$. In the present work, all values related to membrane area are referred to 1μF of its capacitance.

In the present study, we have decided to model the measurement of membrane impedance by investigation of current responses (the total ionic current, i_{ion}, and its components: the fast sodium current, i_{Na}, the time-independent potassium current, i_{K1}, the time-dependent potassium current, i_{x1}, and the slow inward current, i_s) of a cellular mebrane resulting from AC voltage excitations. This procedure (*viz.* analysing a current response to voltage excitation rather than a voltage response to current excitation) allows us to analyse each ionic current separately.

Since we are interested in phenomena occuring in the resting state of the membrane and in all phases of the action potential, the applied voltage excitation is composed of an AC probing voltage and a slowly changing voltage related to the "natural" shape of the action potential. Simulations with such voltage excitation will be called measurement simulations. To obtain a shape of the action potential, an additional reference simulation using current excitation is performed.

Thus, we can consider the differences between currents flowing in the measurement and the reference simulation as responses to an AC test voltage:

$$\begin{bmatrix} \Delta i_{\mathrm{Na}} \\ \Delta i_{\mathrm{K1}} \\ \Delta i_{x1} \\ \Delta i_s \end{bmatrix} = \begin{bmatrix} i_{\mathrm{Na}} \\ i_{\mathrm{K1}} \\ i_{x1} \\ i_s \end{bmatrix}_{\text{measurement}} - \begin{bmatrix} i_{\mathrm{Na}} \\ i_{\mathrm{K1}} \\ i_{x1} \\ i_s \end{bmatrix}_{\text{reference}}, \tag{1}$$

$$\Delta i_{\mathrm{ion}} = \Delta i_{\mathrm{Na}} + \Delta i_{\mathrm{K1}} + \Delta i_{x1} + \Delta i_s, \tag{2}$$

where difference signals Δi_{ion}, Δi_{Na}, Δi_{K1}, Δi_{x1}, Δi_s are respectively: the difference total ionic current, the fast sodium current, the time-independent potassium current, the time-dependent potassium current and the slow inward current.

2.2. Difference signal generation

We perform one reference and a few measurement simulations. The period of 800 ms is analysed, corresponding to a typical full cycle of the heart's activity. All simulations are performed with a time step of $\Delta t = 0.1\,\mu$s.

The reference current excitation simulation is performed as shown in Figure 1. The stimulus current is given as a rectangular pulse of 10 ms width and $10\,\mu\mathrm{A}/\mu\mathrm{F}$ in amplitude. The membrane produces an action potential as a response. The stimulus current and the action potential are shown in Figure 2.

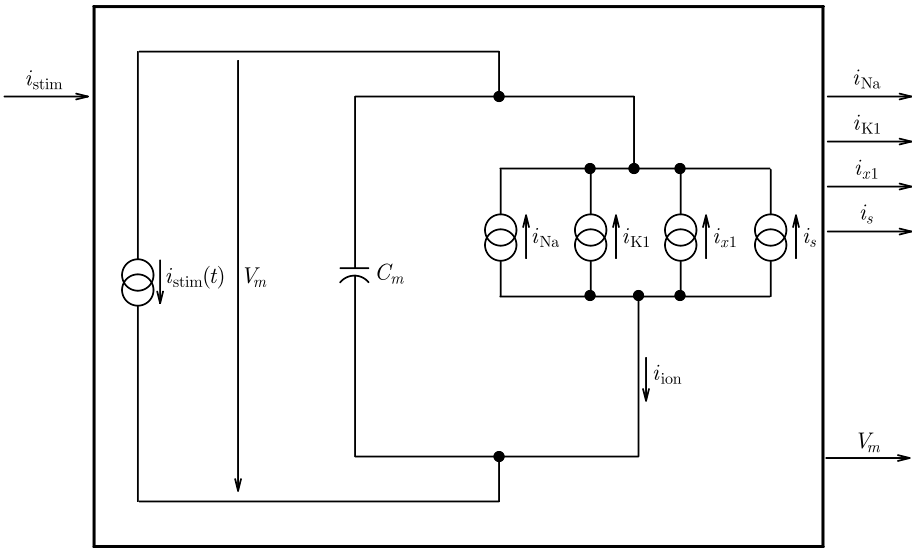

Figure 1. Reference simulation using current excitation: the diagram inside the rectangle shows the simulated electrical circuit, the arrows outside the rectangle show the input and output data of the simulation

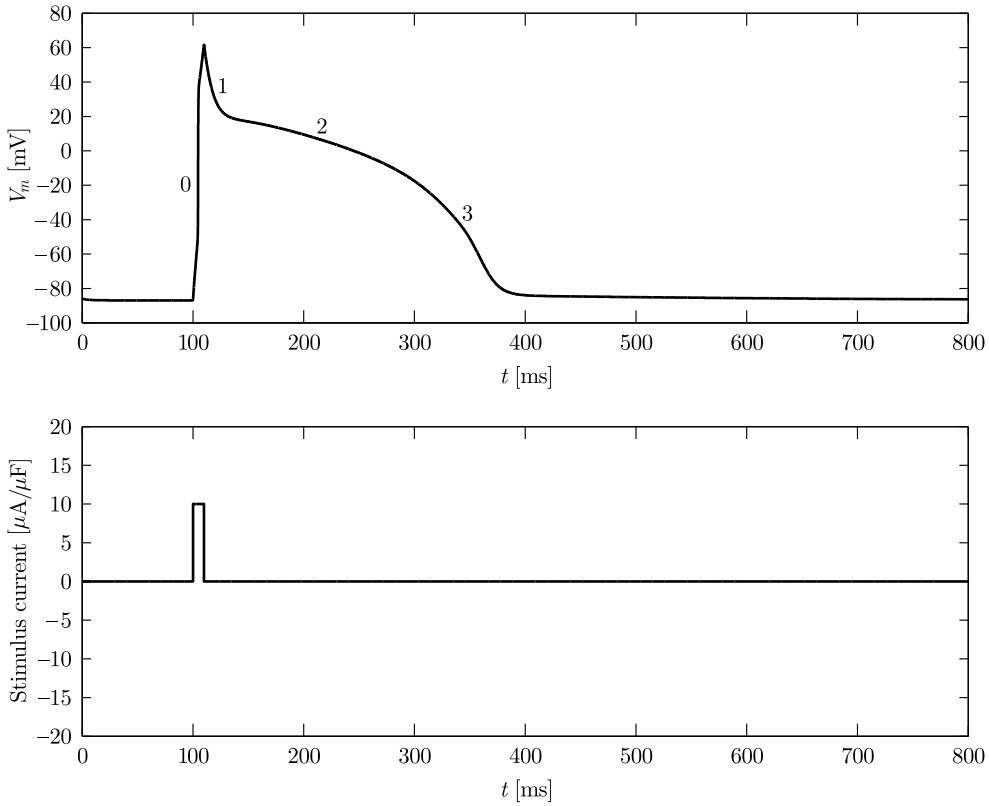

Figure 2. Current stimulus and action potential: digits over the upper line denote phases of the action potential

In the measurement simulation we apply a voltage excitation to the cell membrane, composed of the previously computed reference transmembrane potential and test AC voltage (Figure 3). The sum of these two components is passed as input data to the simulation and is denoted as $V_m(t)$ in the circuit diagram in Figure 3. The total ionic current, i_{ion}, and its components i_{Na}, i_{K1}, i_{x1}, i_s are taken from the simulation as the response. We perform four measurement simulations with different test signals. The frequency, f_x, of the sinusoidal test voltage is set at 1kHz or 100kHz and its RMS value – at 1mV or 10mV.

2.3. Difference signal processing

Each difference signal (1) and (2) is processed in the same way. Three logical channels (Figure 4 shows the architecture of one channel) are applied, each designed to detect and calculate the Root Mean Square value (RMS) of the fundamental frequency and its second and third harmonics.

The core of the channel is a bandpass filter with the middle frequencies of f_x, $2f_x$ and $3f_x$, in order to detect the basic frequency and its second and third harmonics, respectively. We use a finite impulse response filter with a kernel of 751 samples in length. In order to obtain the RMS value of the difference signal, the output of the filter is squared and then filtered again in the Moving Average Filter of the length

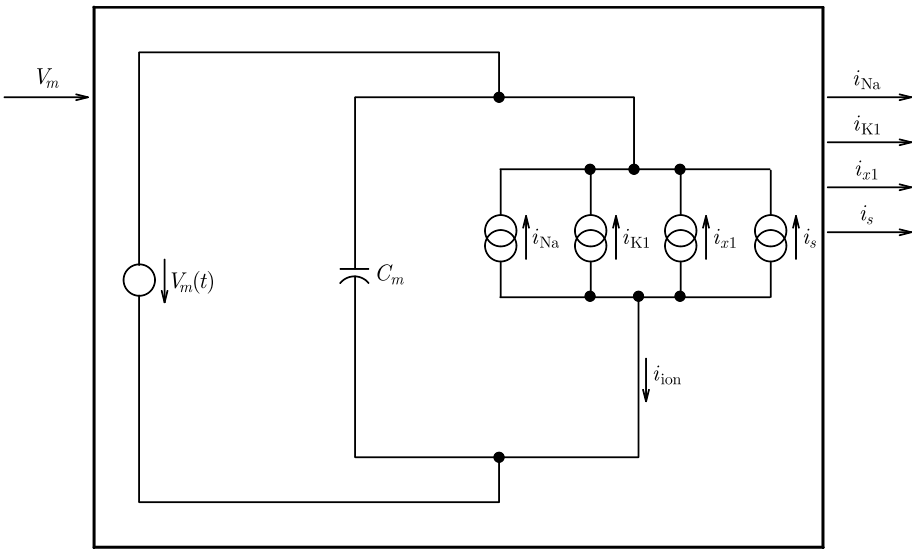

Figure 3. Measurement simulation using voltage excitation: the diagram inside the rectangle shows the simulated electrical circuit, the arrows outside the rectangle show the input and output data of the simulation

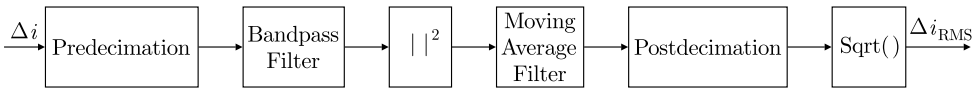

Figure 4. Block diagram of a detection channel

equal to the period of the probing voltage. The square root of the moving average is then used as the RMS value of a particular difference signal.

The difference signal coming from the simulation with 1 kHz probing voltage is decimated (predecimation at the block diagram) by a factor of 100 : 1 before entering the bandpass filter. This procedure allows us to use exactly the same bandpass filters (with 0.01, 0.02 and 0.03 middle normalized frequencies) for both probing frequencies.

Just out of the Moving Average Filter, the signal is decimated, if needed (postdecimation at the block diagram), to the sampling frequency of 100 kHz in order to reduce the data size.

Such design of the detecting channels helps to achieve a compromise between the filter characteristics, both in the time and the frequency domains. Good performance in the frequency domain is obviously necessary to separate the fundamental frequency and the second and third harmonics. At the same time, our design limits the length of filter response to 7.51 ms for the 100 kHz sampling frequency. This allows us to detect rapid changes of the amplitude of the analysed signal.

3. Limitations

There are some limitations of our study. The first comes from the BRDR model used for modelling the membrane kinetics. Since this model is based mainly on voltage clamp experiments, its applicability at high frequencies is not well known

yet. Our results show an important role of the time-independent potassium current in the non-linear response. Therefore, the Luo-Rudy model [9], describing this current more accurately, might be preferable. Neverthless, the BRDR model has already been adapted by Skoubine *et al.* [6] to large, non-physiological values of transmembrane potential, which can be used for measurements. However, we do not use this feature in the present study.

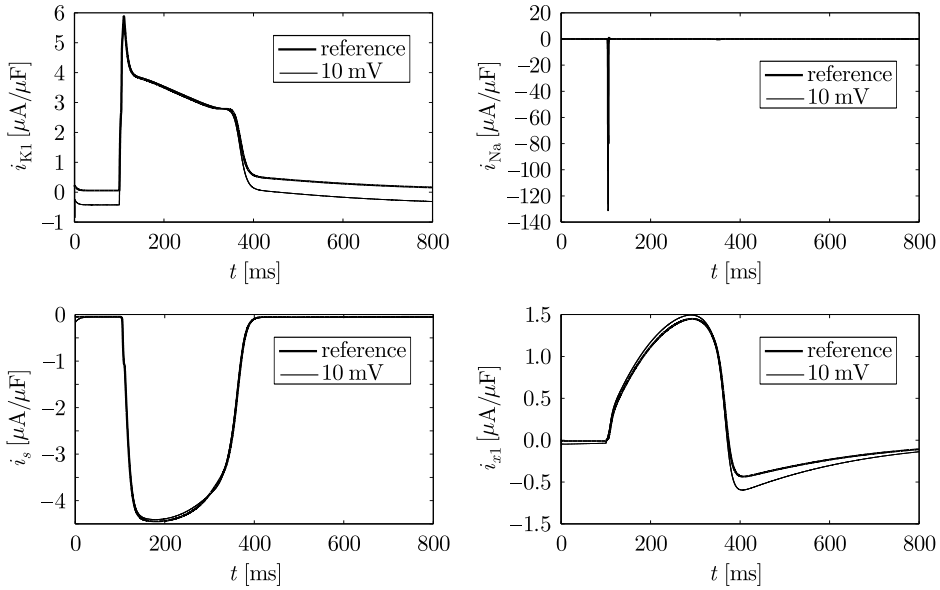

Figure 5. Slowly changing components of all the ionic currents

Another limitation comes from the effect of probing voltage on the slowly changing component of the i_{K1} potassium current (see Figure 5). This effect may not be negligible because of an important role of i_{K1} in the repolarization and determation of the resting potential. The influence of probing voltage on the action potential must be evaluated *in vivo*.

Unfortunately, measurement of non-linear effects in real experiments is difficult. The relatively low level of harmonic distortions produced by the cellular membrane requires a very precise, low-noise measurement equipment with extremely good linearity. The non-linear properties of measurement electrodes can make real measurements very difficult [10].

Since our calculations are performed with double precision and the input data have a similar order of magnitude (-100 mV to 100 mV for the physiological transmembrane potential and about millivolts for the AC test voltage), we assume round-off errors to be negligible.

An analysis of the integration errors is more complex. Simulations without AC performed earlier [11], with an even larger time step, are cosidered to be accurate. Only computations of the time-independent current are obviously unaffected by the integration errors.

It is easy to find that the approximated solution produced in the measurement simulation for a given transmembrane potential is the exact solution for the input transmembrane potential affected by a disturbance not exceeding ΔV_m. The values of ΔV_m, which depend on the possible rate of voltage changes, are presented in Table 1. This limitation of error may be satisfactory for a computation of responses at the fundamental frequency, but not for the second and the third harmonic frequencies.

Table 1. Input transmembrane potential disturbance

Probing voltage		Disturbance ΔV_m
Frequency f_x	RMS	
[kHz]	[mV]	[mV]
100	10	1
100	1	0.1
1	10	0.05
1	1	0.04

A strict analysis of the errors affecting the time-dependent potassium current, the fast sodium current and the slow inward current is difficult due to the complexity of the analytical solution. For instance, for the gating variable m the analytical solution can be written as:

$$m(t) = m_0 \cdot e^{-\varphi_m(t)} + e^{-\varphi_m(t)} \cdot \int \frac{m_\infty(t)}{\tau_m(t)} \cdot e^{\varphi_m(t)} dt, \tag{3}$$

where

$$\varphi_m(t) = \int_0^t \frac{1}{\tau_m(t)} dt \tag{4}$$

and m_0 is a constant. A consideration of measurement simulations in terms of digital signal processing offers a premise to neglect the integration errors. From a DSP viewpoint these simulations can be thought of as a system with a Nyquist frequency of 5 MHz, corresponding to $\Delta t = 0.1\,\mu$s, producing a set of currents as an output from V_m entering its input. Since the input frequency is at least 50 times smaller than the Nyquist frequency, we assume the output currents to be computed accurately. Relatively small levels of harmonic frequencies in the calculated responses confirm this assumption.

4. Results

The four ionic currents i_{Na}, i_{K1}, i_{x1} and i_s are filtered through the Moving Average Filter of 1 ms length and are decimated by a factor of $100:1$ in order to obtain the slowly changing component, which is plotted vs time in Figure 5. The thick lines denote currents recorded from the reference simulation and the thin lines – those from the measurement simulation using 10 mV probing voltage at both frequencies.

The comparison between reference and measurement currents in Figure 5 shows that the applied 10 mV probing voltage affects these currents only slightly during the action potential. However, there is a significant effect on both the time-independent and the time-dependent potassium current when the cell is resting.

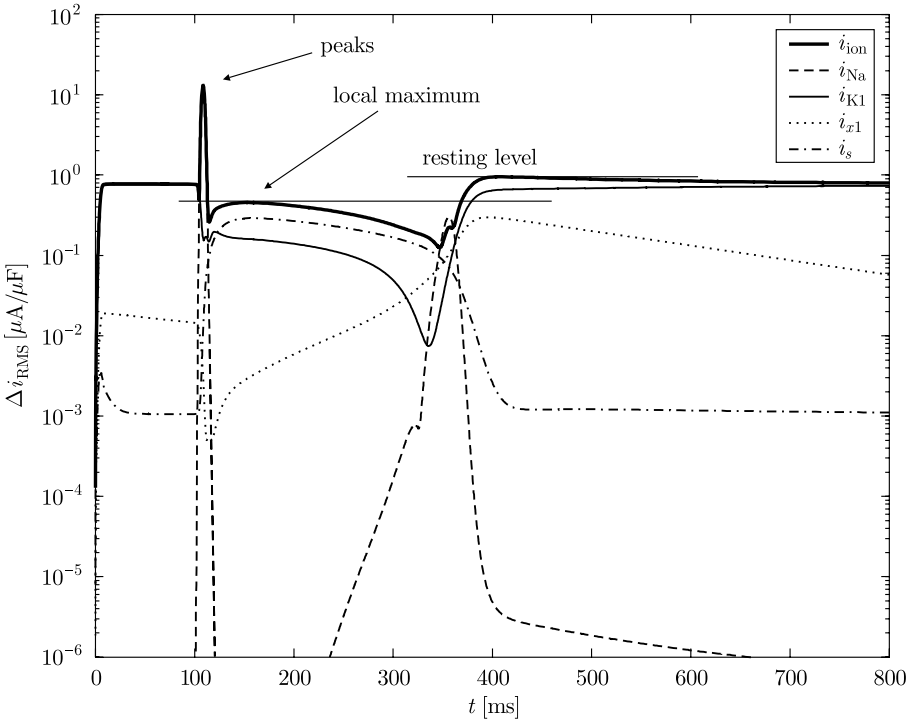

Figure 6. AC response at the fundamental frequency for test voltage 1kHz/10mV

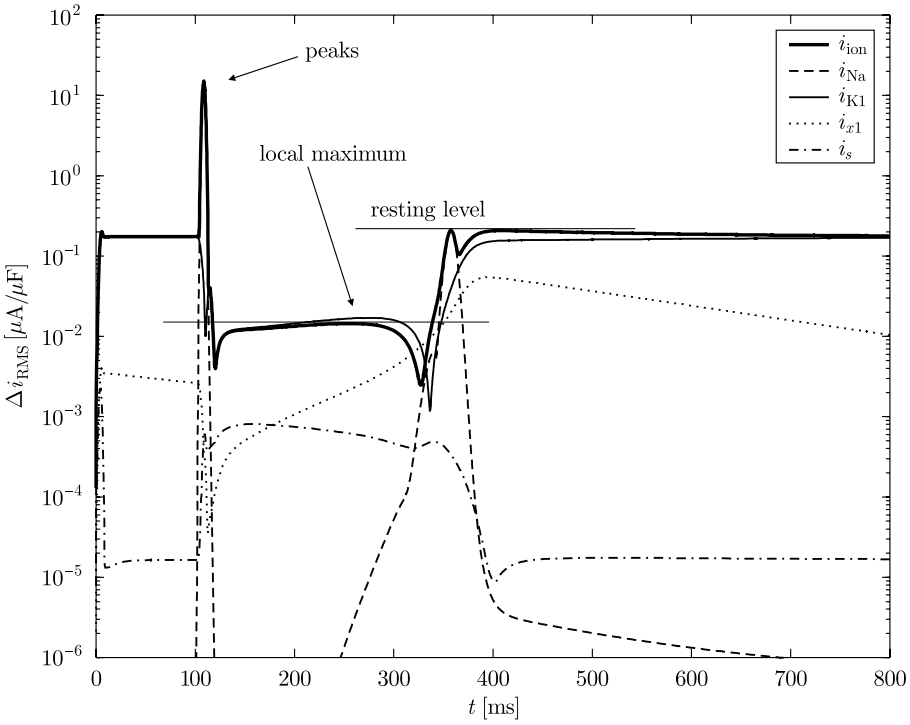

Figure 7. AC response at the second harmonic frequency for test voltage 1kHz/10mV

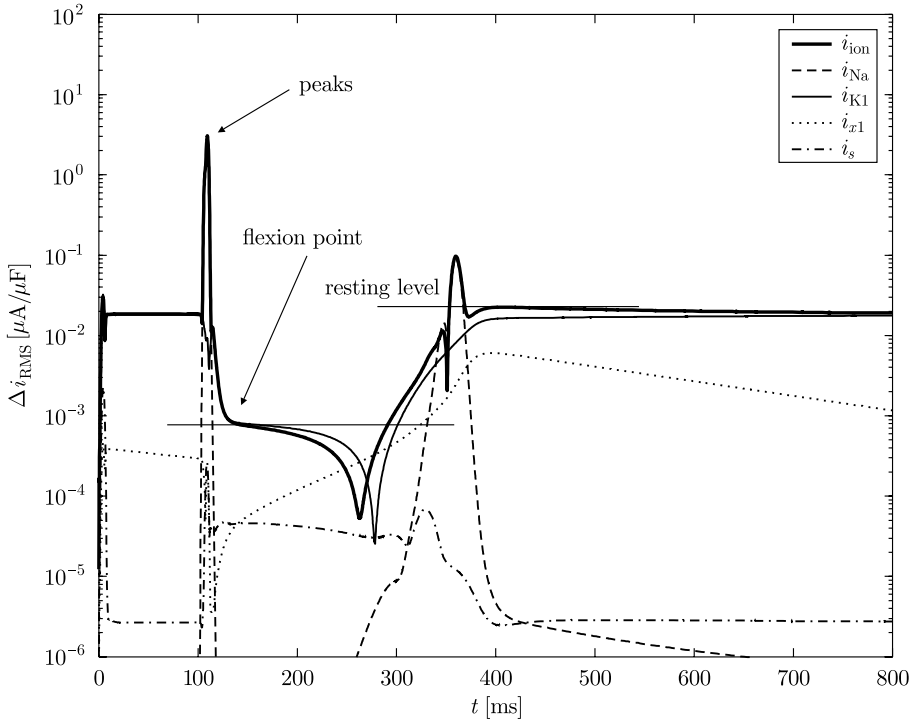

Figure 8. AC response at the third harmonic frequency for test voltage 1kHz/10mV

In Figures 6, 7 and 8, the RMS values of the total ionic current, $i_{\rm ion}$, and its components are plotted at the fundamental and its second and third harmonic frequencies, respectively. We show the results only for the 1kHz/10mV probing signal, which has produced the largest harmonic distortion among all the calculated examples. The shape of the total ionic current is similar for all the examined frequencies. One can distinguish a resting level, a set of positive and negative peaks associated with phases 0 and 1 of the action potential, and a minimum level at the end of the repolarization phase. In addition, there is a plateau during the action potential in the response at the second harmonic frequency.

The responses are at the same level for both probing frequencies. When the probing voltage is increased from 1 to 10mV, the response at the fundamental frequency increases about 10 times, about 100 times at the second harmonic frequency and about 1000 times at the third harmonic frequency, what appears to be reasonable.

The decomposition of the total ionic current into four components shows that the response is mainly contributed to by the time-independent potassium current ($i_{\rm K1}$) when the cell is resting. However, during the action potential, the composition of the total ionic current is more complex. At the fundamental frequency, for both probing voltages, and at the third harmonic frequency for the 1mV voltage, the slow inward current (i_s) transitory constitutes the largest share of the response. Lastly, at the end of the repolarization, the fast sodium current produces a relatively large response, especially for the 1kHz probing frequency.

The minimum of the total ionic current at the fundamental and the second harmonic frequency occurs when the transmembrane potential is about −35 mV, approximately 230 ms after the action potential began. Only at the third harmonic frequency for the 10 mV test voltage this minimum occurs earlier, approximately 160 ms after the action potential began.

For a quantitative description of response variability during the action potential, we define a ratio between the resting level of the response and its local maximum, as presented in Figures 6, 7 and 8. (At the second and third harmonic frequencies the level of plateau or the flexion point is used instead of a local maximum.) The ratio is about 6.5 dB at the fundamental frequency and 22 dB at the second harmonic, independently of the probing signal's voltage or frequency. At the third harmonic this ratio is about 13 dB for the 1 mV probing voltage and 32 dB for the 10 mV test voltage, again regardless of the probing signal's frequency.

5. Discussion and conclusions

A closer look at the charts in Figures 6, 7 and 8 will reveal that the total ionic current is smaller than its components under some conditions (*viz.* the second harmonic response for the 1 kHz/10 mV test voltage). This can be easily explained by a negative dynamic resistance in the characteristics of the slow inward current i_s.

Similarly, the flat region in the current-voltage characteristics of the i_{K1} current is responsible for a minimum of the response near the end of repolarization.

We should also mention the response from the fast sodium current at the termination phase of the action potential. It is relatively high, although the averaged value of this current is small. Information about the state of fast sodium current channels may be very important, considering the role of new action potential initiation during the period of relative refractory in arrhythmogenesis.

The peaks observed at the start of the action potential at all the examined frequencies must be interpreted very carefully. A signal entering the detection channel (Figure 4) contains a step of the i_{K1} current. Therefore, the peaks shown in the AC response graphs may be treated as artifacts produced by the detection channels.

A comparison of the non-linear (see Figures 6, 7 and 8) and the linear responses (presented in Table 2) shows that the variability of the non-linear response at the fundamental frequency is relatively small. Table 2 also shows the admittance corresponding to the total ionic current (non-linear response) at the fundamental frequency and the admittance corresponding to the capacitance current (linear response). As one can see, the admittance related to the ionic current does not depend on the value of probing voltage used. The value of this admittance is less than 1.3% of the capacitative admittance, even for the 1 kHz frequency. This confirms that non-linear effects are small and that the approximation of the membrane as a linear, parallel RC circuit may be sufficient for many applications. Our value of admittance responsible for the ionic current (0.08 mS/μF), corresponding to a 12.5 k$\Omega\cdot$cm^2 specific membrane resistance, is similar to the values presented in other papers [12].

Responses at the third harmonic frequency change over 30 dB for the 10 mV testing voltage, carrying information about the action potential. The 1 kHz/10 mV probing voltage could be the choice for future 3D simulations and real experiments,

Table 2. RMS of current responses

Probing voltage		Linear response from membrane capacitance	Resting level of the non-linear response at frequency			Harmonic distortion level	Admittance related to the capacitance current	Admittance related to the ionic current
f_x	RMS		f_x	$2f_x$	$3f_x$			
[kHz]	[mV]	[μA/μF]	[μA/μF]	[μA/μF]	[μA/μF]	[%]	[mS/μF]	[mS/μF]
100	10	6280.00	0.8	0.2	0.02	0.0032	628.00	0.08
100	1	628.00	0.08	0.002	0.00002	0.00032	628.00	0.08
1	10	62.80	0.8	0.2	0.02	0.32	6.28	0.08
1	1	6.28	0.08	0.002	0.00002	0.032	6.28	0.08

producing the largest and the most variable harmonic distortions, though other probing signals, not tested in the present study, may produce even larger harmonic distortions.

Reverting to the questions asked in the introduction to this paper, we can conclude that in our simulations, for all four examined probing signals:

1. The cardiomyocyte membrane can produce harmonic distortions of up to 0.32%.
2. the changes of the membrane's admittance caused by the action potential do not exceed 1.3%.
3. The 1kHz/10mV probing voltage yields the highest values of harmonic distortions.

Our software is designed for a more general, three-dimensional simulation of the electrical activity of the heart. It has been implemented in serial and parallel versions capable of running on SMP and distributed memory machines using MPI for interprocess communication. The code is being tested on a 128-processor Intel Pentium cluster. Achieving good speed-ups allows us to consider a three-dimensional tissue block instead of merely a piece of a membrane discussed in the present paper.

Acknowledgements

Calculations were carried out at the TASK Academic Computer Center in Gdansk.

Appendix: Model equations

The equations of the BRDR model in its defibrillation version [4–6] are shown below. In this version of the BRDR model, there are alternative formulas introduced for large absolute values of the transmembrane potential. The formulas for relatively low absolute values of the transmembrane potential remain unchanged.

In our study the absolute values of transmembrane potential are relatively low and both versions of the model are equivalent.

The presented equations are recalled from the literature [4–6].

We skip measurement units in the formulas to present the equations in a compact form. Please bear in mind that all currents are expressed in microampers per microfarad, potentials – in millivolts, time – in milliseconds and concetrations – in millimoles per liter.

A1. Fast sodium current

The fast sodium current is given by the following equation:

$$i_{\mathrm{Na}}(t) = G_{\mathrm{Na}} m^3(t) h(t) (V_m(t) - E_{\mathrm{Na}}), \tag{A1}$$

where $G_{\mathrm{Na}} = 15\,\mathrm{mS}/\mu\mathrm{F}$ is the maximum sodium channel conductance, $E_{\mathrm{Na}} = 40\,\mathrm{mV}$ is the sodium equilibrium potential, and m, h are dimensionless gating variables defined as:

$$\frac{dm}{dt} = \alpha_m \cdot (1-m) - \beta_m \cdot m = \frac{m_\infty - m}{\tau_m}, \tag{A2}$$

$$m_\infty = \frac{\alpha_m}{\alpha_m + \beta_m}, \tag{A3}$$

$$\tau_m = \frac{1}{\alpha_m + \beta_m}, \tag{A4}$$

$$\frac{dh}{dt} = \alpha_h \cdot (1-h) - \beta_h \cdot h = \frac{h_\infty - h}{\tau_h}, \tag{A5}$$

$$h_\infty = \frac{\alpha_h}{\alpha_h + \beta_h}, \tag{A6}$$

$$\tau_h = \frac{1}{\alpha_h + \beta_h}, \tag{A7}$$

where the infinity symbol in the subscript denotes the steady state value of a particular gating variable and the letters τ, α, β denote respectively: the time constant and the opening and the closing rate of the gate. Both forms (one with the steady-state value and the time constant, the other with the opening and closing rates) are equivalent. The opening and closing rates are calculated as:

$$\alpha_m = \begin{cases} 890.9437890 \cdot \dfrac{\exp(0.0486479(V_m - 100.0))}{1.0 + 5.93962526 \cdot \exp(0.0486479(V_m - 100.0))} & \text{for } V_m > 100.0, \\ 0.9 \cdot \dfrac{V_m + 42.65}{1.0 - \exp(-0.22(V_m + 42.65))} & \text{for } V_m \le 100.0, \end{cases} \tag{A8}$$

$$\beta_m = \begin{cases} 1.437 \cdot \exp(-0.085(V_m + 39.75)) & \text{for } V_m > -85.0, \\ \dfrac{100.0}{1.0 + \exp(0.2597504(V_m + 85.0))} & \text{for } V_m \le -85.0, \end{cases} \tag{A9}$$

$$\alpha_h = \begin{cases} 0.1 \cdot \exp(-0.193(V_m + 79.65)) & \text{for } V_m > -90.0, \\ -12.0662845 - 0.1422598 V_m & \text{for } V_m \le -90.0, \end{cases} \tag{A10}$$

$$\beta_h = \frac{1.7}{1.0 + \exp(-0.095(V_m + 20.5))}. \tag{A11}$$

A2. Time-dependent potassium current

The time-dependent potassium current is defined by the following equation:

$$i_{x1}(t) = x_1(t) \cdot 0.8 \cdot \frac{\exp(0.04 \cdot (V_m + 77.0)) - 1}{\exp(0.04 \cdot (V_m + 35.0))}, \tag{A12}$$

where x_1 is a dimensionless gating variable:

$$\frac{dx_1}{dt} = \alpha_{x1} \cdot (1 - x_1) - \beta_{x1} \cdot x_1 = \frac{x_{1\infty} - x_1}{\tau_{x1}}, \tag{A13}$$

$$x_{1\infty} = \frac{\alpha_{x1}}{\alpha_{x1} + \beta_{x1}}, \tag{A14}$$

$$\tau_{x1} = \frac{1}{\alpha_{x1} + \beta_{x1}}, \tag{A15}$$

where the infinity symbol in the subscript denotes the steady state value of the gating variable and the letters τ, α, β denote respectively: the time constant, the opening and the closing rate of the

gate. Both forms (one with the steady-state value and the time constant, the other with the opening and closing rates) are equivalent. The opening and closing rates are calculated as:

$$\alpha_{x1} = \begin{cases} \dfrac{151.7994692 \cdot \exp(0.0654679(V_m - 400.0))}{1.0 + 151.7994692 \cdot \exp(0.0654679(V_m - 400.0))} & \text{for } V_m > 400.0, \\ 0.0005 \cdot \dfrac{\exp(0.083(V_m + 50.0))}{1.0 + \exp(0.057(V_m + 50.0))} & \text{for } V_m \leq 400.0, \end{cases} \tag{A16}$$

$$\beta_{x1} = 0.0013 \cdot \frac{\exp(-0.06(V_m + 20.0))}{1.0 + \exp(-0.04(V_m + 20.0))}. \tag{A17}$$

A3. Time-independent potassium current

This current depends only on the transmembrane potential and equals:

$$i_{\mathrm{K1}}(t) = 0.35 \cdot \left(\frac{4.0 \cdot (\exp(0.04(V_m + 85.0)) - 1)}{\exp(0.08(V_m + 53.0)) + \exp(0.04(V_m + 53.0))} + \frac{0.2(V_m + 23.0)}{1 - \exp(-0.04(V_m + 23.0))} \right). \tag{A18}$$

A4. Slow inward current

The slow inward current is carried mainly by calcium ions and is given by the following equation:

$$i_s(t) = G_s d(t) f(t) (V_m(t) - E_s(t)), \tag{A19}$$

where $G_s = 0.09\,\mathrm{mS}/\mu\mathrm{F}$ is the maximum channel conductance, E_s is the equilibrium potential for calcium ions, and d, f are dimensionless gating variables. E_s is considered as changing in time because of the changing intracellular concentration of calcium ions:

$$E_s(t) = 7.7 - 13.0287 \cdot \ln([\mathrm{Ca}]_{\mathrm{i}}(t)), \tag{A20}$$

where $[\mathrm{Ca}]_{\mathrm{i}}$ is intracellular concentration of calcium ions, expressed in $\mathrm{mmol \cdot dm^{-3}}$. This concentration changes according to the following equation:

$$\frac{d[\mathrm{Ca}]_{\mathrm{i}}}{dt} = \begin{cases} 0.0 & \text{for } V_m > 200.0, \\ 0.0001 \cdot i_s(t) + 0.07 \cdot (0.0001 - [\mathrm{Ca}]_{\mathrm{i}}(t)) & \text{for } V_m \leq 200.0. \end{cases} \tag{A21}$$

The gating variables are governed by the equations:

$$\frac{dd}{dt} = \frac{\alpha_d}{R} \cdot (1 - d) - \beta_d \cdot d = \frac{d_\infty - d}{\tau_d}, \tag{A22}$$

$$d_\infty = \frac{\alpha_d / R}{\alpha_d / R + \beta_d}, \tag{A23}$$

$$\tau_d = \frac{1}{\alpha_d / R + \beta_d}, \tag{A24}$$

$$\frac{df}{dt} = \frac{\alpha_f}{R} \cdot (1 - f) - \beta_f \cdot f = \frac{f_\infty - f}{\tau_f}, \tag{A25}$$

$$f_\infty = \frac{\alpha_f / R}{\alpha_f / R + \beta_f}, \tag{A26}$$

$$\tau_f = \frac{1}{\alpha_f / R + \beta_f}, \tag{A27}$$

where the infinity symbol in the subscript denotes the steady-state value of the gating variable and the letters τ, α, β denote respectively: the time constant, the opening and the closing rate of the gate. R is a dimensionless parameter allowing one to model prolongation of the action potential; in the present study we have assumed $R = 1$. Both forms (one with the steady-state value and the time

constant, the other with the opening and closing rates) are equivalent. The opening and closing rates are calculated as:

$$\alpha_d = \frac{0.095 \cdot \exp(-0.01 \cdot (V_m - 5.0))}{1.0 + \exp(-0.072 \cdot (V_m - 5.0))}, \tag{A28}$$

$$\beta_d = \frac{0.07 \cdot \exp(-0.017 \cdot (V_m + 44.0))}{1.0 + \exp(0.05 \cdot (V_m + 44.0))}, \tag{A29}$$

$$\alpha_f = \frac{0.012 \cdot \exp(-0.008 \cdot (V_m + 28.0))}{1.0 + \exp(0.15 \cdot (V_m + 28.0))}, \tag{A30}$$

$$\beta_f = \frac{0.0065 \cdot \exp(-0.02 \cdot (V_m + 30.0))}{1.0 + \exp(-0.2 \cdot (V_m + 30.0))}. \tag{A31}$$

A5. Model implementation

Application of the BRDR model leads to the following set of ordinary differential equations with V_m, m, h, x_1, d, f, $[\mathrm{Ca}]_\mathrm{i}$ as unknowns:

$$\begin{cases} \dfrac{dV_m}{dt} = \dfrac{i_\mathrm{ion} + i_\mathrm{stim}}{C_0} \\ \dfrac{dm}{dt} = \alpha_m \cdot (1-m) - \beta_m \cdot m = \dfrac{m_\infty - m}{\tau_m}, \\ \dfrac{dh}{dt} = \alpha_h \cdot (1-h) - \beta_h \cdot h = \dfrac{h_\infty - h}{\tau_h}, \\ \dfrac{dx_1}{dt} = \alpha_{x1} \cdot (1-x_1) - \beta_{x1} \cdot x_1 = \dfrac{x_{1\infty} - x_1}{\tau_{x1}}, \\ \dfrac{dd}{dt} = \dfrac{\alpha_d}{R} \cdot (1-d) - \beta_d \cdot d = \dfrac{d_\infty - d}{\tau_d}, \\ \dfrac{df}{dt} = \dfrac{\alpha_f}{R} \cdot (1-f) - \beta_f \cdot f = \dfrac{f_\infty - f}{\tau_f}, \\ \dfrac{d[\mathrm{Ca}]_\mathrm{i}}{dt} = \begin{cases} 0.0 & \text{for } V_m > 200.0, \\ 0.0001 \cdot i_s(t) + 0.07 \cdot (0.0001 - [\mathrm{Ca}]_\mathrm{i}(t)) & \text{for } V_m \le 200.0, \end{cases} \end{cases} \tag{A32}$$

where $C_0 = 1\,\mu\mathrm{F}/\mu\mathrm{F}$ is a unitary capacitance.

The numerical approximation of the solution is denoted with a *tilde* over the letter and is computed from the following:

$$\begin{cases} \widetilde{V}_m(t+\Delta t) = \widetilde{V}_m(t) + \Delta t \cdot \dfrac{\widetilde{i}_\mathrm{ion}(t) + \widetilde{i}_\mathrm{stim}(t)}{C}, \\ \widetilde{m}(t+\Delta t) = \widetilde{m}(t) + (\widetilde{m}_\infty(t) - \widetilde{m}(t)) \Big(1 - \exp\Big(\dfrac{-\Delta t}{\widetilde{\tau}_m(t)}\Big)\Big) = \widetilde{m}_\infty(t) - (\widetilde{m}_\infty(t) - \widetilde{m}(t)) \cdot \exp\Big(\dfrac{-\Delta t}{\widetilde{\tau}_m(t)}\Big), \\ \widetilde{h}(t+\Delta t) = \widetilde{h}(t) + (\widetilde{h}_\infty(t) - \widetilde{h}(t)) \Big(1 - \exp\Big(\dfrac{-\Delta t}{\widetilde{\tau}_h(t)}\Big)\Big), \\ \widetilde{x}_1(t+\Delta t) = \widetilde{x}_1(t) + (\widetilde{x}_{1\infty}(t) - \widetilde{x}_1(t)) \Big(1 - \exp\Big(\dfrac{-\Delta t}{\widetilde{\tau}_{x1}(t)}\Big)\Big), \\ \widetilde{d}(t+\Delta t) = \widetilde{d}(t) + (\widetilde{d}_\infty(t) - \widetilde{d}(t)) \Big(1 - \exp\Big(\dfrac{-\Delta t}{\widetilde{\tau}_d(t)}\Big)\Big), \\ \widetilde{f}(t+\Delta t) = \widetilde{f}(t) + (\widetilde{f}_\infty(t) - \widetilde{f}(t)) \Big(1 - \exp\Big(\dfrac{-\Delta t}{\widetilde{\tau}_f(t)}\Big)\Big), \\ [\widetilde{\mathrm{Ca}}]_\mathrm{i}(t+\Delta t) = [\widetilde{\mathrm{Ca}}]_\mathrm{i}(t) + \Delta t \cdot \begin{cases} 0.0 & \text{for } \widetilde{V}_m(t) > 200.0, \\ 0.0001 \cdot \widetilde{i}_s(t) + 0.07 \cdot (0.0001 - [\widetilde{\mathrm{Ca}}]_\mathrm{i}(t)) & \text{for } \widetilde{V}_m(t) \le 200.0. \end{cases} \end{cases} \tag{A33}$$

References

[1] Cinca J, Warren M, Carreno A, Tresanchez M, Armadans L, Gomez P and Soler-Soler J 1997 *Circulation* **96** (9) 3079

[2] Drazner M H, Thompson B, Rosenberg P B, Kaiser P A, Boehrer J D, Baldwin B J, Dries D L and Yancy C W 2002 *Am. J. Cardiol.* **89** (8) 993
[3] Hodgkin A L and Huxley A F 1952 *J. Physiol.* **117** (4) 500
[4] Beeler G W and Reuter H 1977 *J. Physiol.* **268** (1) 177
[5] Drouhard J P and Roberge F A 1987 *Comput. Biomed. Res.* **20** (4) 333
[6] Skouibine K B, Trayanova N A and Moore P K 1999 *IEEE Trans. Biomed. Eng.* **46** (7) 769
[7] Luo C H and Rudy Y 1994 *Circ. Res.* **74** (6) 1071
[8] Luo C H and Rudy Y 1994 *Circ. Res.* **74** (6) 1097
[9] Luo C H and Rudy Y 1991 *Circ. Res.* **68** (6) 1501
[10] Richardot A and McAdams E T 2002 *IEEE Trans. Med. Imaging* **21** (6) 604
[11] Huiskamp G 1998 *IEEE Trans. Biomed. Eng.* **45** (7) 847
[12] Muzikant A L and Henriquez C S 1998 *IEEE Trans. Biomed. Eng.* **45** (4) 449